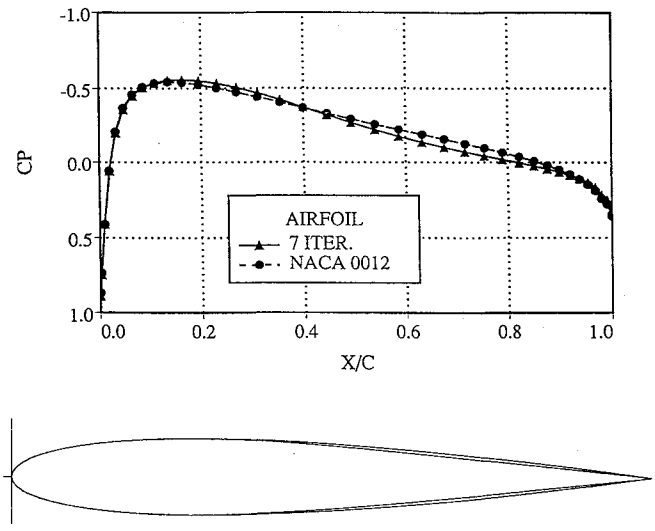

Fig. 3 Pressure distributions and shapes of design and target airfoils.

directional searches. The parallel optimization scheme used central-difference estimations of the derivatives for the calculation of each component of the gradient vector. The sequential optimization scheme first attempted forward-difference estimations of the derivatives because less objective function evaluations were required. When the directional search used by QNMDIF did not reduce the objective function based upon the forward-difference estimation of the gradient, QNMDIF then recomputed central-difference estimations and conducted additional directional searches. This resulted in great inefficiencies for the sequential airfoil design test case.

The parallel line search was more efficient in reducing the objective function than the sequential line search. The minimum variation for the directional search was determined by the value of the estimated machine precision, and the maximum variation of the thickness was set to 1% chord to ensure only small perturbations of the airfoil shape. The sequential line search evaluated a maximum of eight objective functions in each direction of search. The parallel line search was more thorough than the sequential search because it evaluated 16 objective functions in the direction of search including the maximum and minimum points.

The final shape of the design airfoil using PARQNM is shown with the NACA 0012 target airfoil with their resulting pressure distributions in Fig. 3. The design airfoil's shape is nearly identical to the target airfoil from the leading edge to the point of maximum thickness where the greatest changes in pressure occur.

Conclusions

This work applies recent advances in parallel supercomputing technology to an intuitively parallel problem. Through the use of parallel supercomputers, applications of optimization methods based upon gradient methods are faster and more efficient. The parallel optimization routine performs second-order-accurate gradient estimations and more thorough directional searches in parallel that increases the speed and the efficiency of the quasi-Newton routine. For the particular case of airfoil design via optimization that requires multiple calculations of expensive objective functions, the utilization of the parallel quasi-Newton routine can result in design solutions many times faster than with a sequential optimization routine.

References

[1]Kennelly, R. A., "Improved Method for Transonic Airfoil Design-by-Optimization," AIAA Paper 83-1864, Jan. 1983.

[2]Verhoff, A., Stookesberry, D., and Cain, A., "An Efficient Approach to Optimal Aerodynamic Design, Part 1: Analytic Geometry and Aerodynamic Sensitivities," AIAA Paper 93-0099, Jan. 1993.

[3]Brawley, S. C., "Aerodynamic Design Using Parallel Processors," Ph.D. Dissertation, U.S. Naval Postgraduate School, Monterey, CA, Sept. 1993.

[4]Sorenson, R. L., "A Computer Program to Generate Two-Dimensional Grids About Airfoils and Other Shapes by the Use of Poisson's Equation," NASA TM-81198, May 1980.

Analytical Expression of Induced Drag for a Finite Elliptic Wing

Masami Ichikawa*
Okayama Prefectural University, Okayama-ken 719-11, Japan

Introduction

THE two available formulas for calculating induced drag for a thin wing differ in their physical concepts. One is called the near field and the other is the far field. Since both equations agree with each other in the thin wing theory, induced drag calculations by these formulas have been used to examine numerical planar lifting-surface methods.[1,2] Most of these lifting-surface methods have only demonstrated the agreement of two kinds of induced drags, but have not addressed the accuracy of predicted induced drags. For example, Wagner's result for a variable-sweep wing shows a good agreement, but its predicted distribution for the sectional induced drag is excessively wavy.[3] Until now, analytical verifications have been unavailable for even a circular wing in incompressible flow.[4] Recently, the author has obtained such solutions by using Kida's method.[5] This Note shows the procedure for obtaining analytical solutions of the induced drag of an elliptic wing in incompressible steady flow, based on linearized theory. Furthermore, some numerical results are presented.

Formulation

Reference 5 gives the exact lifting-surface solution of the elliptic wing shown in Fig. 1 using the acceleration potential. This solution consists of two parts: one is the solution for the wing of the geometrical parameter k, defined in Fig. 1, less than unity, and the other is that for wing of larger than unity. Only the former case is discussed here.

Far-Field Induced Drag Solution

The total induced drag D_i acting on a wing surface is estimated by the following relation:

$$D_i = -\rho \int_{-a}^{+a} \Gamma(x) \cdot w_i(x)\, dx \qquad (1)$$

where ρ denotes the air density, $\Gamma(x)$ is the circulation distribution, and $w_i(x)$ is the induced downwash velocity distribution on the wing surface by a planar wake over the wingspan.

Received Aug. 26, 1995; revision received Dec. 20, 1995; accepted for publication Jan. 5, 1996.

*Assistant Professor, Department of System Engineering.

Table 1 Comparison of the total induced drag coefficient

Method	Circular wing			Elliptic wing, AR = 10		
	C_L	C_{Di}^F	C_{Di}^N	C_L	C_{Di}^F	C_{Di}^N
Present method	1.790	0.801	0.801	5.062	0.816	0.816
Extended lifting-line theory	1.830	0.837	——	5.151	0.845	——
Simple lifting-line theory	2.444	1.493	——	5.236	0.873	——

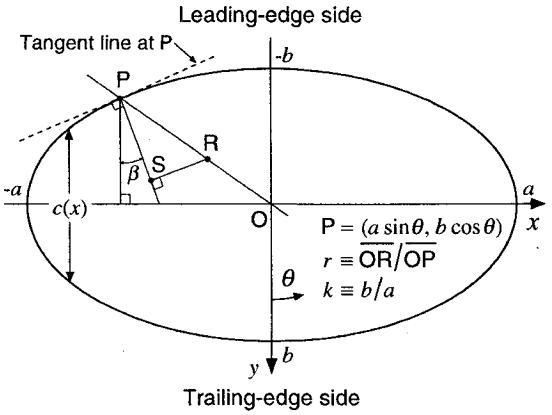

Fig. 1 Coordinates and notation of an elliptic wing.

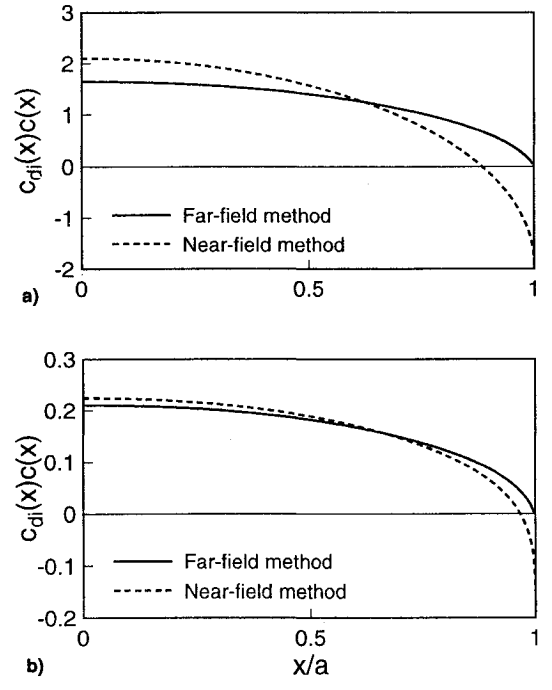

Fig. 2 Sectional induced drag distributions of a) circular and b) elliptic wings.

The induced downwash velocity and the circulation are related by the equation:

$$w_i(x) = -\frac{1}{4\pi}\int_{-a}^{+a}\frac{\frac{\partial\Gamma}{\partial\xi}}{x-\xi}\,d\xi \tag{2}$$

and the circulation $\Gamma(x)$ of the elliptic wing is expressed by[5]

$$\frac{\Gamma(x)}{U} = 2a\pi^2\sum_{n=0}^{\infty} D_n P_{2n}\left(\frac{x}{a}\right) \tag{3}$$

where U denotes the velocity of main flow, and P_{2n} are the Legendre functions of the first kind. The method for determining the coefficients D_n is presented in Ref. 5. Substituting Eqs. (2) and (3) into Eq. (1) yields the total induced drag coefficient:

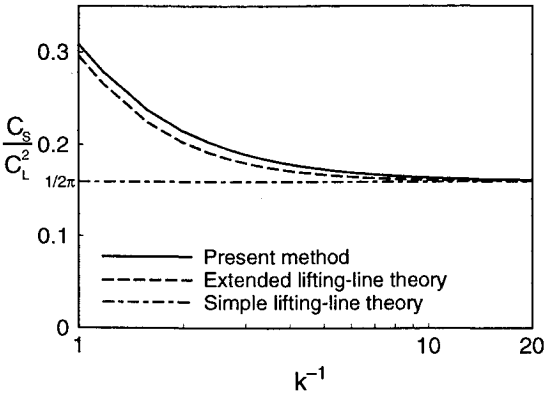

Fig. 3 Total suction force vs the reciprocal of k.

$$C_{Di}^F = \frac{4\pi^2}{k}\sum_{m=0}^{\infty}\sum_{n=1}^{\infty}\sum_{j=1}^{n}\frac{(4j-1)D_mD_n}{(m+j)(2m-2j+1)} \tag{4}$$

where the suffix F denotes the far field. The sectional induced drag coefficient of the far-field method is given by[6]

$$c_{di}^F = \frac{4a\pi^3}{c(x)}\sum_{m=0}^{\infty}\sum_{n=1}^{\infty}\sum_{j=1}^{n}(4j-1)D_mD_nP_{2m}\left(\frac{x}{a}\right)Q_{2j-1}\left(\frac{x}{a}\right) \tag{5}$$

where $c(x)$ is the local chord length expressed by $2b\sqrt{1-x^2/a^2}$, and Q_{2j-1} are the Legendre functions of the second kind. It is noticed that the far-field calculation cannot predict sectional induced drag exactly because of its physical concept.

Near-Field Induced Drag Solution

The near-field induced drag requires the evaluation of the streamwise leading-edge suction force X, which is given by the following expression[7]:

$$X = -\rho\pi C^2(\theta)\cos\beta \tag{6}$$

where $C(\theta)$ is an unknown function and β is the angle shown in Fig. 1. The function $C(\theta)$ is determined by considering the streamwise perturbation velocity u near the leading edge. This velocity at point R on the segment OP in Fig. 1 is given by, using Eq. (6) of Ref. 5,

$$u = \pi A(\theta)/\sqrt{1-r^2} \tag{7}$$

where the reader may refer to Ref. 5 for the details of the function $A(\theta)$. Also, another expression for u at point S in Fig. 1 is given by[7]

$$u = C(\theta)\cos\beta/\sqrt{\overline{PS}} \tag{8}$$

where $\overline{PS} = ab(1-r)/\sqrt{a^2\sin^2\theta + b^2\cos^2\theta}$. Since Eqs. (7)

and (8) should agree with each other in the limit when r approaches unity, the following result is obtained:

$$C(\theta) = \pi\sqrt{b/a}(a^2 \cos^2\theta + b^2 \sin^2\theta)^{1/4}A(\theta)/\cos\theta \quad (9)$$

Once the function $C(\theta)$ has been determined, the sectional suction force coefficient becomes

$$c_s = -\pi^3\sqrt{\cos^2\theta + k^2 \sin^2\theta}A^2(\theta)/2\cos^3\theta \quad (10)$$

and the total suction force coefficient is

$$C_S = -2\pi^2 \int_{\pi/2}^{\pi} \frac{\sqrt{\cos^2\theta + k^2 \sin^2\theta}A^2(\theta)}{\cos\theta}\,d\theta \quad (11)$$

Hence, the sectional induced drag coefficient is given by $c_{di}^N = c_l\alpha - c_s$, and the total induced drag coefficient by $C_{Di}^N = C_L\alpha - C_S$. The suffix N denotes the near field, c_l is the sectional lift coefficient, C_L is the total lift coefficient, and α is the angle of attack. The definite integral in Eq. (11) is evaluated numerically, and the lift coefficients are calculated from Eq. (3).

Numerical Results

In numerical examples α is assumed to be 1 rad. Table 1 shows a comparison study of the total induced drag between the present method and two kinds of lifting-line theories.[8] Two lifting-line theories are unable to predict the near-field induced drag. This result confirms the validity of the present analysis because the agreement of two kinds of induced drags is good. Figures 2a and 2b show the spanwise distributions of the sectional induced drags by the present analysis for the cases of Table 1. The sectional distributions of two methods are different near the wingtip of even the large aspect ratio elliptic wing.

Figure 3 shows a comparison result of the total suction force for various values of k. Even the extended lifting-line theory will not estimate induced drag sufficiently at the values of k above about 0.25, that is, of an aspect ratio below about 6.4.

Conclusions

This Note has presented analytical solutions for two kinds of induced drag calculations describing circular and elliptic wings in linearized incompressible steady flow using Kida's method. Good agreement between two kinds of induced drags shows the validity of the present analysis. Moreover, it is shown that the sectional distributions of two kinds of induced drags are different in the case of even the large aspect ratio elliptic wing. Those solutions will be useful in the examination of numerical lifting-surface theories.

References

[1]Kalman, T. P., Giesing, J. P., and Rodden, W. P., "Spanwise Distribution of Induced Drag in Subsonic Flow by the Vortex Lattice Method," *Journal of Aircraft*, Vol. 7, No. 2, 1970, pp. 574–576.

[2]Lan, C. E., "A Quasi-Vortex-Lattice Method in Thin Wing Theory," *Journal of Aircraft*, Vol. 11, No. 9, 1974, pp. 518–527.

[3]Wagner, S., "On the Singularity Method of Subsonic Lifting-Surface Theory," *Journal of Aircraft*, Vol. 6, No. 6, 1969, pp. 549–558.

[4]Medan, R. T., "Improvements to the Kernel Function Method of Steady Subsonic Lifting Surface Theory," NASA TM X-62, 327, March 1974.

[5]Kida, T., "A Theoretical Treatment of Lifting Surface Theory of an Elliptic Wing," *ZAMM*, Vol. 60, 1980, pp. 645–651.

[6]Katz, J., and Plotkin, A., *Low-Speed Aerodynamics: From Wing Theory to Panel Methods*, McGraw–Hill, New York, 1991, Chap. 8.

[7]Robinson, A., and Laurmann, J. A., *Wing Theory*, Cambridge Univ. Press, London, 1956, Chap. 3.

[8]Schlichting, H., and Truckenbrodt, E., *Aerodynamic of the Airplane*, McGraw–Hill, New York, 1979, Chap. 3.

Determination of Aircraft Stall Margins During Takeoff

Sergey Kofman* and Georges A. Bécus†
University of Cincinnati, Cincinnati, Ohio 45221-0070

Nomenclature

C_D = coefficient of drag
C_L = coefficient of lift
$C_{L\max}$ = lift coefficient corresponding to stall angle of attack
$C_{L\text{peak}}$ = lift coefficient corresponding to peak angle of attack
C_m = coefficient of pitching moment
$\bar{c}$ = mean aerodynamic chord, m
D = drag force, N
f = coefficient of friction
H = altitude, m
I_{yy} = Y-body axis moment of inertia, kg-m^2
L = lift force, N
M = aircraft total moment, N-m
M_a = aircraft aerodynamic moment, N-m
M_g = moment generated by landing gears, N-m
m = aircraft mass, kg
Q = pitch rate, rad/s
$\bar{q}$ = dynamic pressure, N/m^2
R_g = normal reaction on the landing gears, N
S = wing planform area, m^2
T = thrust force, N
V = calibrated airspeed, m/s
V_S = calibrated stalling speed, m/s
W = aircraft weight, N
x_{cg} = center of gravity
x_{ac} = aerodynamic center
α = angle of attack, rad
α_{peak} = maximum angle of attack, reached during the maneuver, rad
α_{stall} = stall angle of attack, rad
γ = flight-path angle, rad
δ_{el} = elevator deflection, rad
$\delta_{\text{l.e.}}$ = leading-edge device deflection, rad
θ = pitch angle, rad
φ_{eng} = thrust vector angle, rad

Introduction

THE problem of change in aircraft performance because of different configurations (malfunctioning of the control system can leave trailing-edge flaps or leading-edge devices in an inadequate position), as well as various flight conditions, receives considerable theoretical and practical attention during aircraft design, flight tests, and certification. The evaluation of variations in stall characteristics and overall aircraft performance because of an inadequate takeoff configuration is important from a safety standpoint. In the past, several accidents (Northwest DC-9, Detroit[1] and Delta B-727, Dallas[2]) have been associated with an improperly set takeoff configuration (inadvertent flaps-up).

Existing Federal Aviation Regulations (FAR)[3] define stall speed V_S as a calibrated stalling speed or the minimum steady flight speed, in knots, at which the aircraft is controllable, with several conditions, specified in FAR §25.103. Stall margin can

Received March 5, 1995; revision received Oct. 12, 1995; accepted for publication Oct. 17, 1995.

*Graduate Student, Aerospace Engineering and Engineering Mechanics. Student Member AIAA.

†Associate Professor, Aerospace Engineering and Engineering Mechanics. Senior Member AIAA.